



# Formation process of a two-dimensional starting jet

Haojun Zheng<sup>1</sup> , Lei Gao<sup>2</sup>  and Simon C.M. Yu<sup>1</sup> 

<sup>1</sup>Department of Aeronautical and Aviation Engineering, The Hong Kong Polytechnic University, Kowloon, Hong Kong, PR China

<sup>2</sup>School of Aeronautics and Astronautics, Sichuan University, Chengdu 610065, PR China

**Corresponding author:** Lei Gao, [lei.gao@scu.edu.cn](mailto:lei.gao@scu.edu.cn)

(Received 18 May 2024; revised 3 October 2024; accepted 13 December 2024)

---

The formation process of a vortex pair generated by a two-dimensional starting jet has been investigated numerically over a range of Reynolds numbers from 500 to 2000. The effects of stroke ratio and nozzle configuration are examined. Only a single vortex pair can be observed in the vorticity field generated by small stroke ratios less than 10 while the leading vortex pair formed by larger stroke ratios eventually disconnects from the trailing jet. The formation numbers (13.6 and 9.3) for a straight nozzle and an orifice nozzle have been identified by the circulation criterion and they are further analysed by four other criteria. Using the contraction coefficient, formation numbers can be transformed into a universal value at about 16.5 for both nozzles. The effect of Reynolds number on the formation number is found to be within 12 % for parallel flow cases but it will increase up to 27 % for non-parallel flow cases due to shear-layer instability. A modified contraction-based slug model is proposed, and it can accurately predict the total invariants (e.g. circulation, hydrodynamic impulse and kinetic energy) shedding from the nozzle edge. Analytical estimation of the formation number is further conducted by matching the predicted total invariants to the Pierrehumbert model of steady vortex pairs. By assuming that pinch-off starts when the vortex pair achieves the steady state, two analytical models are proposed in terms of vortex impulse and translational velocity. The latter appears to be more appropriate to predict the formation number for two-dimensional flows.

**Key words:** vortex dynamics, jets

---

## 1. Introduction

Vortices play important roles in the behaviour of complex flows in nature due to their relevance to many basic components of transitional and turbulent flows. For example, a counter-rotating vortex pair appearing in the wake of an air vehicle attracts the attention

of investigators due to the potential hazard to the vehicles behind (Lewke, Le Dizes & Williamson 2016). A two-dimensional vortex pair consisting of equal but opposite vorticity can be theoretically modelled by two rectilinear line vortices of equal and opposite circulation.

Gharib, Rambod & Shariff (1998) discovered a critical stroke ratio (i.e.  $L/D$ , where  $L$  is the stroke length and  $D$  is the nozzle diameter) at around 4 in starting axisymmetric jets. They defined this universal time as the formation number and explained the onset of vortex ring pinch-off process using the Kelvin–Benjamin variational principle. Pinch-off happens when the vortex generator is no longer able to deliver energy to the leading vortex ring at a sufficient rate with the requirement that the translating vortex ring reaches a steady state of maximum kinetic energy. In addition to the dynamical discussion of vortex invariants (e.g. circulation, hydrodynamic impulse and kinetic energy), the appearance of pinch-off can also be explained by the kinematic manifestation (Shusser & Gharib 2000) and the instability in trailing shear layers (Zhao, Frankel & Mongeau 2000; Gao & Yu 2012). As a result, vorticity accumulating in the trailing jet is absent eventually when the stroke ratio is smaller than the formation number but is present when the stroke ratio is larger than the formation number. This physical phenomenon has also been discussed in various scenarios (Dabiri & Gharib 2004; Ai *et al.* 2005; Allen & Naitoh 2005; Gao *et al.* 2008; Fernando & Rival 2016; Gao & Yu 2016*b*; Fernández & Sesterhenn 2017). It is noted that the influence on the formation number is limited for a broad range of Reynolds numbers from 500 to 5000 (Rosenfeld *et al.* 1998, 2009). The appearance of Kelvin–Helmholtz instabilities in the trailing jet would accelerate vortex pinch-off and thereby reduce the formation number slightly (Zhao *et al.* 2000). Almost all formation numbers found in experiments lie in the range from 3.6 to 4.5 (at about  $4 \pm 0.4$ ) over a wide range of flow conditions (Gharib *et al.* 1998).

A vortex pinch-off in general was not observed in two-dimensional starting jets. In the experimental studies of vortex dipoles (Afanasyev 2006) at Reynolds numbers of the order of  $10^2$ , a clear pinch-off was not observed up to a stroke ratio of 15 in the vorticity field and 51 in flow visualization studies. In the numerical study of orifice-generated vortex pairs (Pedrizzetti 2010) at a Reynolds number of 2000, a tendency for the leading vortex to detach from the trailing shear layer was not observed. The longitudinal size of the leading vortex was found to increase linearly up to a stroke ratio of 12.

Several studies have attempted to explain the absence of pinch-off in the formation of a vortex pair. From the perspective of the kinematic argument, Pedrizzetti (2010) attributed the reason to a lower translational velocity for the leading vortex than that for the trailing shear layer. Similarly, Domenichini (2011) found that the curvature effect could induce a faster moving vortex ring than a vortex pair. Subsequently, O’Farrell & Dabiri (2012) demonstrated that the stability of the leading vortex is important to pinch-off because vortex shedding was not observed in the two-dimensional family of Pierrehumbert vortex pairs subjected to a prolate perturbation. Gao & Yu (2016*a*) suggested that shear-layer instability would be more appropriate to explain the pinch-off of a vortex pair. Sadri & Krueger (2016) not only confirmed the effect of vortex line curvature but also suggested that the lack of vortex stretching may lead to the absence of pinch-off in the formation of a vortex pair. The aforementioned studies indicate that the two-dimensional vortex pair cannot in general satisfy the Kelvin–Benjamin variational principle.

However, the steady vortex pair has been theoretically shown to be at a state of the maximum kinetic energy for a given hydrodynamic impulse (Arnold 1965). This implies that the vortex pinch-off originally discovered in starting axisymmetric flows should be theoretically feasible in two-dimensional flows. Thomson (1880) suggested that a vortex should be in a state of maximum kinetic energy for a given circulation and hydrodynamic

impulse if the motion is steady and stable. The existence of extremal kinetic energy therefore should be the result of the stability problem for steady Euler flows. Kelvin's variational principle was mathematically proven by Arnold (1965). It was suggested that a steady and stable solution for a class of two-dimensional incompressible inviscid flows is the extremal of the kinetic energy with respect to the iso-vortical perturbations. More details for this conclusion for a two-dimensional vortex pair can be found in previous discussions (Turkington 1983; Saffman 1992). Subsequently, extending to one of the simplest three-dimensional flows, Benjamin (1976) verified the Kelvin–Benjamin variational principle for an axisymmetric vortex ring moving steadily in an inviscid incompressible fluid. This flow was found to be at the maximum state of the kinetic energy with a constraint of constant hydrodynamic impulse. From the statistical equilibrium theory for two-dimensional flows as a Hamiltonian system, the final equilibrium state (i.e. a state of maximizing entropy with constraints on invariants of motion) of axisymmetric inviscid flows would satisfy the energy extremization in Kelvin's variational principle (Mohseni 2001). Recently, motivated by the works of Vallis, Carnevale & Young (1989) and Shepherd (1990), Flierl & Morrison (2011) proposed a numerical algorithm to obtain the stationary states of energy extrema in two-dimensional Euler flows at fixed Casimir invariants. These findings generally suggest that a state of maximum energy would also exist in the leading vortex of two-dimensional starting jets.

A pressure-based mechanism was used to identify the pinch-off process in unsteadily axisymmetric jets (Lawson & Dawson 2013; Schlueter-Kuck & Dabiri 2016). This method was found to be comparable to the Lagrangian coherent structure analysis. When the leading vortex ring grew near to the formation number, a trailing pressure maximum (i.e. the rear stagnation point) appeared behind the vortex core. This rear high-pressure region works as a barrier to reject fluids from the trailing jet. As a matter of fact, the rear boundary (i.e. the high-pressure region) would become stronger when the leading vortex ring absorbs more and more vorticity from the trailing jet. This implies that a similar situation may exist for the two-dimensional starting jet.

Afanasyev (2006) mentioned that the pinch-off could be observed at a dimensionless time of 25 in numerical work using the viscous vortex particle method. Experimental (Afanasyev 2006) and numerical (Pedrizzetti 2010) works only investigated the vorticity growth of vortex pairs up to stroke ratios of 15 and 10, respectively. Thus, a larger stroke ratio may be required to further investigate the vortex pair formation.

The main objective of our study is to examine the formation of a vortex pair at large stroke ratios for a detailed investigation of the pinch-off in two-dimensional starting jets. The stroke ratios considered are available over a wide range covering the universal formation number. The nozzle configurations include both straight nozzle and orifice nozzle.

The paper is organized as follows. The numerical set-up, verification and validation are introduced in § 2. The classical and contraction-based slug models are introduced in § 3. To study the critical formation number in two-dimensional flows, both local and global analyses are used and described in § 4. In addition, the influence of Reynolds numbers on the formation number is discussed. In § 5, the differences between two-dimensional and axisymmetric formation numbers are discussed via detailed comparisons. The contraction-based slug model used successfully in axisymmetric flows is modified and used to predict the dynamical invariants of the total jet. In § 6, analytical models based on the vortex impulse and vortex translational velocity are proposed to predict formation numbers for the straight nozzle and orifice nozzle. The paper ends with brief concluding remarks in § 7.

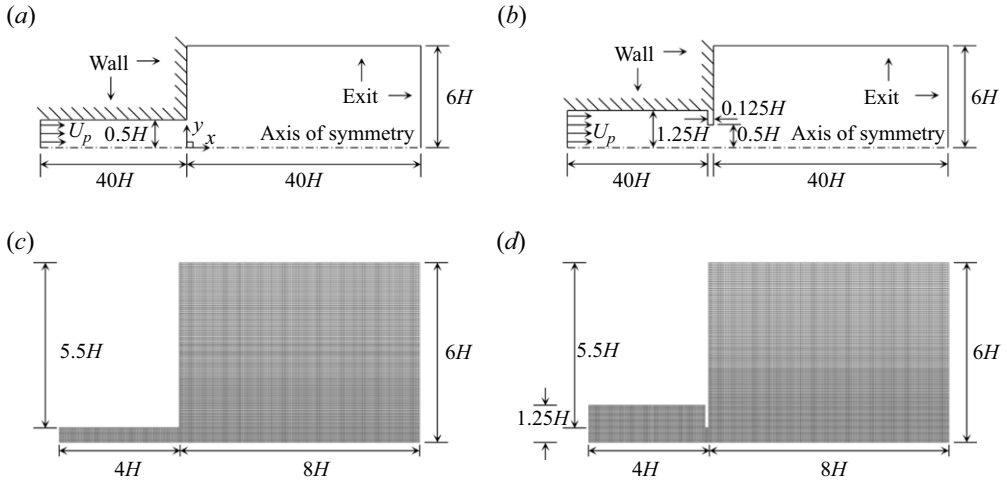


Figure 1. Computational domains (not to scale) for (a) straight nozzle and (b) orifice nozzle. Sample meshes (every sixth mesh point is shown in each direction) for (c) straight nozzle and (d) orifice nozzle.

## 2. Numerical method

### 2.1. Problem statement

The computational domains are presented in figure 1. A fluid column of stroke length  $L(t)$  is pushed through a two-dimensional nozzle with a height  $H$  at the exit plane. The origin of coordinates is located at the centre of the nozzle exit, and the symmetry axis is aligned with the  $x$  direction. The distances from the nozzle exit to the upstream nozzle inlet and downstream exit boundary are both fixed at  $40H$ . The outer boundary is placed at a lateral distance of  $6H$  from the symmetry axis. A squared-off lip at the orifice is used to avoid numerical singularities.

No-slip condition is enforced on the nozzle wall and the outer orifice plate. The pressure outlet with zero gauge pressure is employed on the outer and downstream exits. The piston motion is modelled as a time-dependent velocity inlet boundary (Rosenfeld, Rambod & Gharib 1998; Zhu *et al.* 2023a,b). A uniform velocity profile is specified at the nozzle inlet to control piston velocity  $U_p(t)$ . An impulsive velocity programme at the nozzle exit is defined as

$$U_0(t) \begin{cases} U & \text{for } t \leq \tau, \\ 0 & \text{for } t > \tau, \end{cases} \quad (2.1)$$

where  $U$  is the constant velocity at the nozzle exit and  $\tau$  is the jet discharge time. The maximum stroke length and time-averaged exit velocity are  $L_m = \int_0^\tau U_0 dt = U\tau$  and  $\bar{U}_0 = (\tau)^{-1} \int_0^\tau U_0 dt = U$ . The non-dimensional formation time is defined as  $t^* = \bar{U}_0 t / H$ .

As listed in table 1, a total of 15 cases are simulated. Water is used as the working fluid, with density  $\rho = 998.2 \text{ kg m}^{-3}$  and dynamic viscosity  $\mu = 1.003 \times 10^{-3} \text{ kg m}^{-1} \text{ s}^{-1}$ . The same exit height  $H = 2 \text{ cm}$  and jet velocity  $U = 5 \text{ cm s}^{-1}$  for both the straight nozzle and orifice nozzle provide the same momentum flux at the nozzle exit. To avoid the possible occurrence of Kelvin–Helmholtz instability during jet discharge, a Reynolds number ( $Re_H = \bar{U}_0 H / \nu$ ) of 1000 is chosen for all cases, where  $\nu$  is the kinematic viscosity. The onset of vortex pinch-off for the non-parallel flow cases would occur earlier than for the parallel flow cases (Limbourg & Nedić 2021c). The chosen stroke ratios for the orifice cases should be large enough to study the formation number in the present study.

Case	Geometry	$L_m/H$
SN050	Straight nozzle	5
SN075	Straight nozzle	7.5
SN100	Straight nozzle	10
SN125	Straight nozzle	12.5
SN150	Straight nozzle	15
SN175	Straight nozzle	17.5
SN200	Straight nozzle	20
SN225	Straight nozzle	22.5
SN250	Straight nozzle	25
ON050	Orifice nozzle	5
ON075	Orifice nozzle	7.5
ON100	Orifice nozzle	10
ON125	Orifice nozzle	12.5
ON150	Orifice nozzle	15
ON175	Orifice nozzle	17.5

Table 1. Cases considered.

Therefore, the chosen stroke ratios for orifice cases are slightly smaller than those for cases with the straight nozzle.

### 2.2. Mathematical formulation and numerical method

The two-dimensional, unsteady, incompressible and laminar Navier–Stokes equations are solved by the commercial finite-volume package ANSYS Fluent (version 2020 R1). The pressure-implicit with splitting of operators (PISO) algorithm with the non-iterative time advancement scheme is used for pressure–velocity coupling. Second-order schemes are employed in spatial and temporal discretization. In addition, the passive scalar is computed by solving the convection–diffusion equation. Parameter  $C$  represents the mass fraction concentration of the scalar. The fluids inside and outside the nozzle are defined with  $C = 1$  and  $C = 0$  initially. The inflow at the nozzle inlet is defined with  $C = 1$  during jet discharge. The Schmidt number  $Sc = \nu/\Gamma_c$  is fixed at 1 (Sau & Mahesh 2007), where  $\Gamma_c$  is the scalar diffusivity. The computational domains are discretized by structured meshes. The grid is uniform along the streamwise direction with a spacing  $\Delta x = H/100$ . With an average spacing  $\overline{\Delta y} = H/100$ , the total grid number along the transverse direction is determined. The grids below the height of the nozzle wall are uniform with a refined spacing  $\overline{\Delta y} = H/(100 \times 1.4)$  to capture details in the boundary layer and shear layer. The remanent grids above the height of the nozzle wall are stretched slightly in the transverse direction. High-resolution simulations are employed with  $4001 \times 601$  grid points outside the nozzle. Sample meshes for the straight nozzle and orifice nozzle are partially shown in figures 1(c) and 1(d). The time step is fixed at 0.001 s to ensure that the cell Courant numbers are less than one for all cases.

### 2.3. Verification of numerical method

Cases for respective independent tests are listed in table 2. The tests are evaluated for the streamwise vortex trajectory ( $x_v^* = x_v/H$ ) for cases SN250 and ON175. For the domain-independent tests shown in figure 2(a), the convergence of numerical results can be observed as the domain size increases. The trajectory for the chosen domains deviates less than 2% from that for the larger domains  $40H \times 8H$ . For the grid-independent tests in figure 2(b) and time-step-independent tests in figure 2(c), the numerical results are not

Case	Domain outside nozzle	$\Delta x = \overline{\Delta y}$	Mesh outside nozzle	Total cell number
SN250-SDS	$40H \times 4H$	$H/100$	$4001 \times 401$	$1.9 \times 10^6$
SN250-LDS	$40H \times 8H$	$H/100$	$4001 \times 801$	$3.5 \times 10^6$
SN250-CM	$40H \times 6H$	$H/50$	$2001 \times 301$	$6.7 \times 10^5$
SN050–SN250	$40H \times 6H$	$H/100$	$4001 \times 601$	$2.7 \times 10^6$
SN250-FM	$40H \times 6H$	$H/150$	$6001 \times 901$	$6.0 \times 10^6$
ON175-SDS	$40H \times 4H$	$H/100$	$4001 \times 401$	$2.3 \times 10^6$
ON175-LDS	$40H \times 8H$	$H/100$	$4001 \times 801$	$3.9 \times 10^6$
ON175-CM	$40H \times 6H$	$H/50$	$2001 \times 301$	$7.8 \times 10^5$
ON050–ON175	$40H \times 6H$	$H/100$	$4001 \times 601$	$3.1 \times 10^6$
ON175-FM	$40H \times 6H$	$H/150$	$6001 \times 901$	$7.0 \times 10^6$

Table 2. Grid sizes used for independent tests.

sensitive to the mesh and time-step choices. Comparing with the denser mesh  $6001 \times 901$  or smaller time step  $0.0005$  s, the errors for the developed vortex pair are generally less than 4%. In short, the error and convergence for the present domain size, mesh and time step suggest that the numerical set-up is sufficient to describe the vortex motion adequately. To validate the numerical results, the evolution of the transverse trajectory ( $y_v^* = y_v/H$ ) starting at the nozzle edge is plotted in figure 2(d). The numerical result for the straight nozzle satisfies the 2/3 power law (red dashed line) suggested by the roll-up theory of a two-dimensional vortex sheet developed at the edge of a semi-infinite flat plate (Saffman 1978).

#### 2.4. Vortex invariants and vortex boundary

The main dynamical properties of the two-dimensional vortex motion are the circulation, the hydrodynamic impulse and the kinetic energy. The quantities can be obtained by the area integration inside the vortex core on the upper semi-plane (Batchelor 1967; Saffman 1992), such as

$$\Gamma_v = \int \int \omega \, dx \, dy, \tag{2.2}$$

$$I_v = \rho \int \int y\omega \, dx \, dy, \tag{2.3}$$

$$E_v = \frac{1}{2}\rho \int \int \omega\psi \, dx \, dy, \tag{2.4}$$

where  $\omega$  is the azimuthal vorticity and  $\psi$  is the stream function. It is noted that the integrals of the vortex pair are different from those of the vortex ring (Gharib *et al.* 1998). The cutoff level to determine the vortex core boundary is defined as 5% of the local maximum vorticity (Rosenfeld *et al.* 1998; Zhao *et al.* 2000; Sau & Mahesh 2007). Sensitivity analysis had been made by the cutoff level of 2%. The differences of the vortex invariants are within 3% for both nozzle configurations. Therefore, the vortex invariants are found to be insensitive to the choice of the cutoff level. In addition, the pressure-based method is used to further identify the rear vortex boundary (Lawson & Dawson 2013). The features of the vortex boundary in the pressure field are found to be accurate by comparing with the Lagrangian vortex boundary (Baskaran & Mulleners 2022). Based on

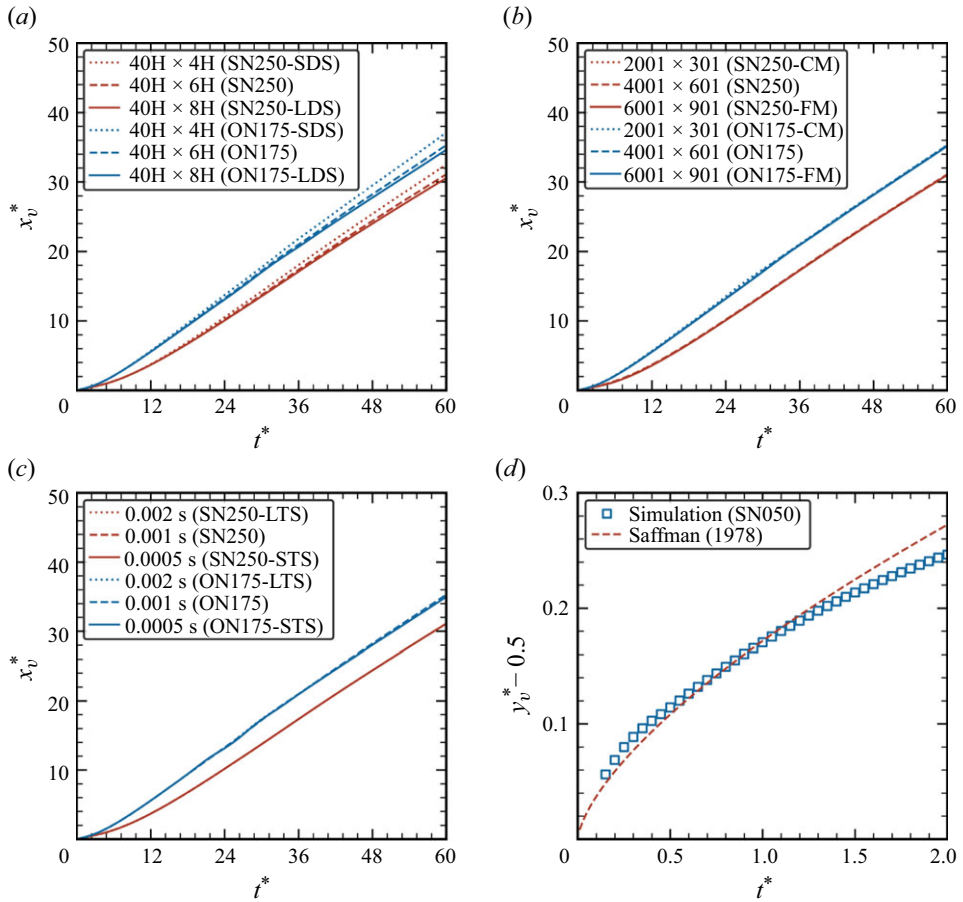


Figure 2. Numerical tests on vortex trajectories for (a) domain sizes, (b) grid sizes and (c) time steps. (d) Validation with Saffman theory. Abbreviations: SDS/LDS, CM/FM and STS/LTS represent small/large domain size, coarser/finer mesh and small/large time step.

the maximum in the centreline pressure, the trailing pressure maximum at the vortex rear boundary is determined along the symmetry axis (e.g. the blue dashed lines in figure 3a, b). Moreover, the vortex centre (red dashed lines) and front boundary (yellow dashed lines) can also be identified by this pressure-based method. This method can locate the rear boundary before a clear vorticity separation appears between the leading vortex and the trailing jet, as shown in figure 3(c). Based on the cutoff of vorticity level together with the pressure-based method, the vortex boundary can be identified over a wide range of non-dimensional time for the calculation of vortex invariants throughout the entire studies.

### 3. Slug model for total invariants

The invariants of the motion were introduced in unbounded inviscid incompressible flows, such as circulation, impulse and energy. The classical slug model was originally developed to predict total circulation shedding from the sharp edge of an axisymmetric straight nozzle

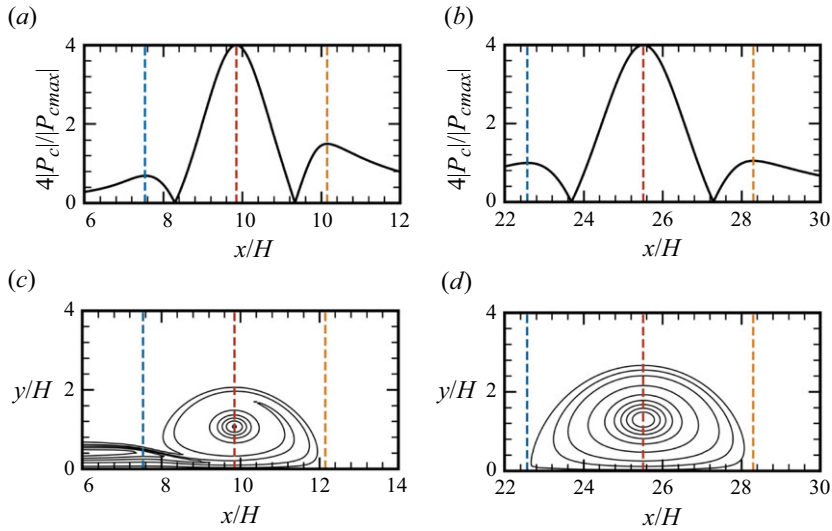


Figure 3. Pressure-based vortex boundary (case SN250). (a,b) The pressure normalized by the maximum and (c,d) the vorticity contours normalized by local maximum (from 0.05 to 1, with 10 levels). Results at (a,c)  $t^* = 20$  and (b,d)  $t^* = 50$ . Blue, red and yellow dashed lines represent the rear, the centre and the front of the vortex.

(Didden 1979). By definition, the rate of circulation change is equal to the vorticity flux at the nozzle exit plane during jet discharge, i.e.

$$\frac{d\Gamma_{slug}}{dt} = \int_0^\infty u_x \omega \, dy = \int_0^\infty u_x \left( \frac{\partial u_y}{\partial x} - \frac{\partial u_x}{\partial y} \right) dy = \int_0^\infty u_x \frac{\partial u_y}{\partial x} dy + \frac{1}{2} U_{outlet}^2, \quad (3.1)$$

where  $U_{outlet}$  is the centreline velocity at the nozzle exit. Considering the uniform assumption of streamwise velocity and the parallel-flow assumption for a straight nozzle, the transverse velocity component  $u_y$  would be zero, leading to an approximated form:

$$d\Gamma_{slug} = \frac{1}{2} U^2 dt. \quad (3.2)$$

This slug model for the total circulation was extended to estimate the hydrodynamic impulse and kinetic energy for a parallel starting jet (Gharib *et al.* 1998), such as

$$dI_{slug} = \frac{1}{4} \pi \rho U^2 D^2 dt, \quad (3.3)$$

$$dE_{slug} = \frac{1}{8} \pi \rho U^3 D^2 dt, \quad (3.4)$$

where  $D$  is the diameter of a circular nozzle. However, this model deviates from the real situation with a time-dependent streamwise velocity profile due to the growth of the boundary layer inside the nozzle (Rosenfeld *et al.* 1998). Thus, this model performs worse at a later time for parallel starting jets. In addition, this model was less successful in the cases of non-parallel flows generated by a circular orifice (Krieg & Mohseni 2013). The reason was attributed to the significant transverse velocity associated with the over-pressure effect at the nozzle exit (Krueger 2005).

To overcome the disadvantage of the slug model in orifice-generated flows, a modification for axisymmetric flows was proposed based on the contraction

coefficient defined at the vena contracta originally for two-dimensional jets (Limbourg & Nedić 2021a). The contraction coefficient is defined as the ratio of the area of the vena contracta  $A_*$  to the area of the nozzle exit  $A$ , such as

$$C_c = \frac{A_*}{A} = \frac{D_*^2}{D^2} = \frac{U}{U_*} = \frac{L}{L_*}. \quad (3.5)$$

According to mass conservation, the quantities at the nozzle exit can be transformed into those at the downstream vena contracta (subscript  $*$ ). The contraction-based slug model for impulsively axisymmetric starting jets can thus be expressed as

$$\Gamma_* = \frac{1}{2}L_*U_* = \frac{1}{2}LU \times 1/C_c^2, \quad (3.6)$$

$$I_* = \frac{1}{4}\pi\rho L_*U_*D_*^2 = \frac{1}{4}\pi\rho LUD^2 \times 1/C_c, \quad (3.7)$$

$$E_* = \frac{1}{8}\pi\rho L_*U_*^2D_*^2 = \frac{1}{8}\pi\rho LU^2D^2 \times 1/C_c^2. \quad (3.8)$$

Determination of the contraction coefficient  $C_c$  for orifice cases was related to the orifice-to-tube diameter ratio (Limbourg & Nedić 2021a). It is noted that this contraction-based model with suggested value  $C_c = 0.9$  was available for parallel flows with considerable boundary layer (Limbourg & Nedić 2021b). Thus, this contraction-based model may be used to predict total invariants for both an axisymmetric straight nozzle and orifice nozzle.

For impulsively two-dimensional flows (Afanasyev 2006), the slug-flow model can be written as

$$\Gamma_{slug2} = \frac{1}{2}LU, \quad (3.9)$$

$$I_{slug2} = \rho LHU, \quad (3.10)$$

$$E_{slug2} = \frac{1}{2}\rho LHU^2. \quad (3.11)$$

With the consideration of contracted flows generated by the two-dimensional orifice nozzle, the two-dimensional slug model can be rewritten as

$$\Gamma_{*2} = \frac{1}{2}L_*U_* = \frac{1}{2}LU \times 1/C_c^2, \quad (3.12)$$

$$I_{*2} = \rho L_*H_*U_* = \rho LHU \times 1/C_c, \quad (3.13)$$

$$E_{*2} = \frac{1}{2}\rho L_*H_*U_*^2 = \frac{1}{2}\rho LHU^2 \times 1/C_c^2, \quad (3.14)$$

where the contraction coefficient follows the relations

$$C_c = \frac{H_*}{H} = \frac{U}{U_*} = \frac{L}{L_*}. \quad (3.15)$$

The slug model (3.9)–(3.11) and the contraction-based slug model (3.12)–(3.14) for two-dimensional flows are evaluated in § 5.

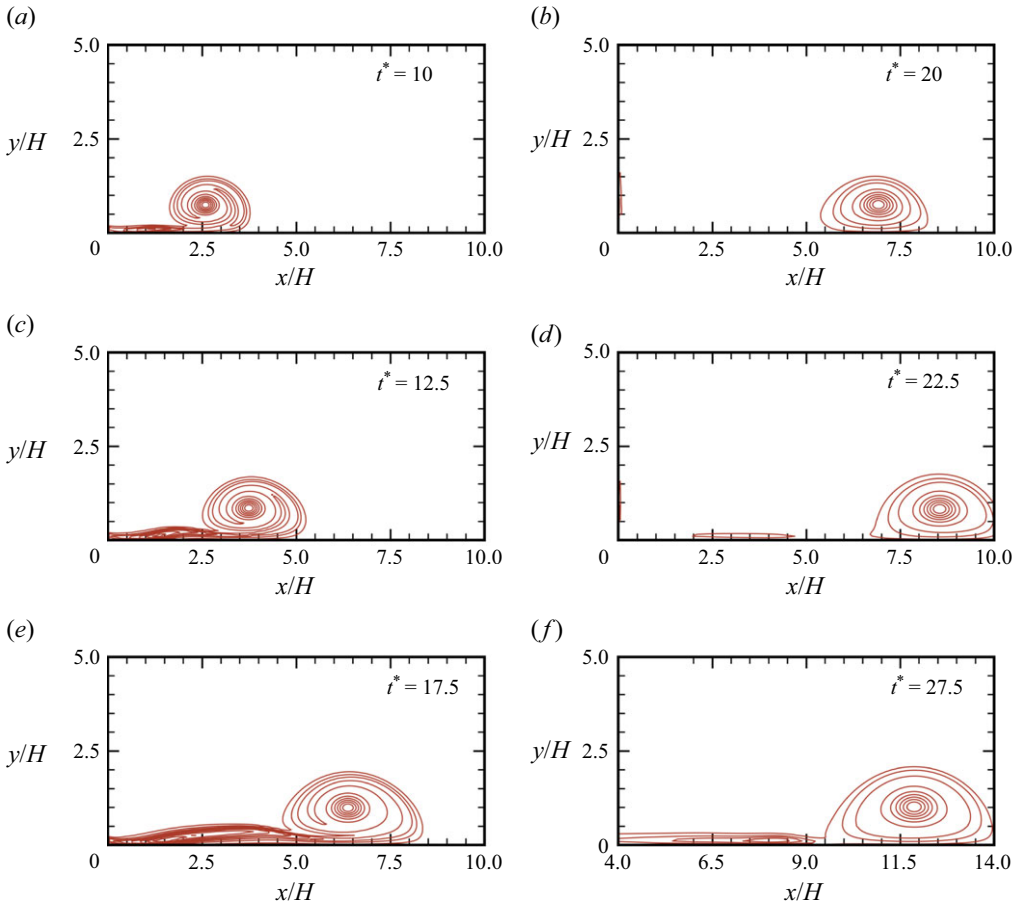


Figure 4. Normalized vorticity fields for the straight nozzle at stroke ratios of (a,b) 7.5, (c,d) 10 and (e,f) 15. The vorticity field has 10 levels from 0.05 to 1.

#### 4. Two-dimensional formation number

According to the definition of critical stroke ratio for the pinch-off process (Gharib *et al.* 1998), the existence of a trailing jet after jet discharge is crucial to describe the maximum energy state of the leading vortex. To examine the effect of stroke ratio on the existence of a trailing jet, comparisons of the vorticity fields at the instant slightly larger than the maximum stroke ratio ( $t^* = L_m/H + 2.5$ ) and at a much later moment ( $t^* = L_m/H + 12.5$ ) are presented in figures 4 and 5 for the straight nozzle and orifice nozzle, respectively. Vorticity fields are normalized by the local maximum. As shown in figures 4(a,c,e) and 5(a,c,e), the starting jet includes a leading vortex ring and a trailing jet without any separations between them at around the maximum stroke ratio. The trailing jet is eventually absent when the stroke ratio is small (see figures 4b and 5b). On the other hand, shear layers separating from the leading vortex pair can be observed in figures 4(d) and 5(d) when the stroke ratio is large. This result implies a critical formation number at around 10 for the two-dimensional starting jets generated by either the straight nozzle or orifice nozzle. With the increase in stroke ratio, the vortex pair grows in size and becomes more difficult to disconnect completely from the trailing jet in the vorticity field (figures 4f and 5f).

The absence of a clear pinch-off in a previous simulation (Pedrizzetti 2010) might be due to the limited stroke ratio (up to 10). As stated in experimental results (Gharib

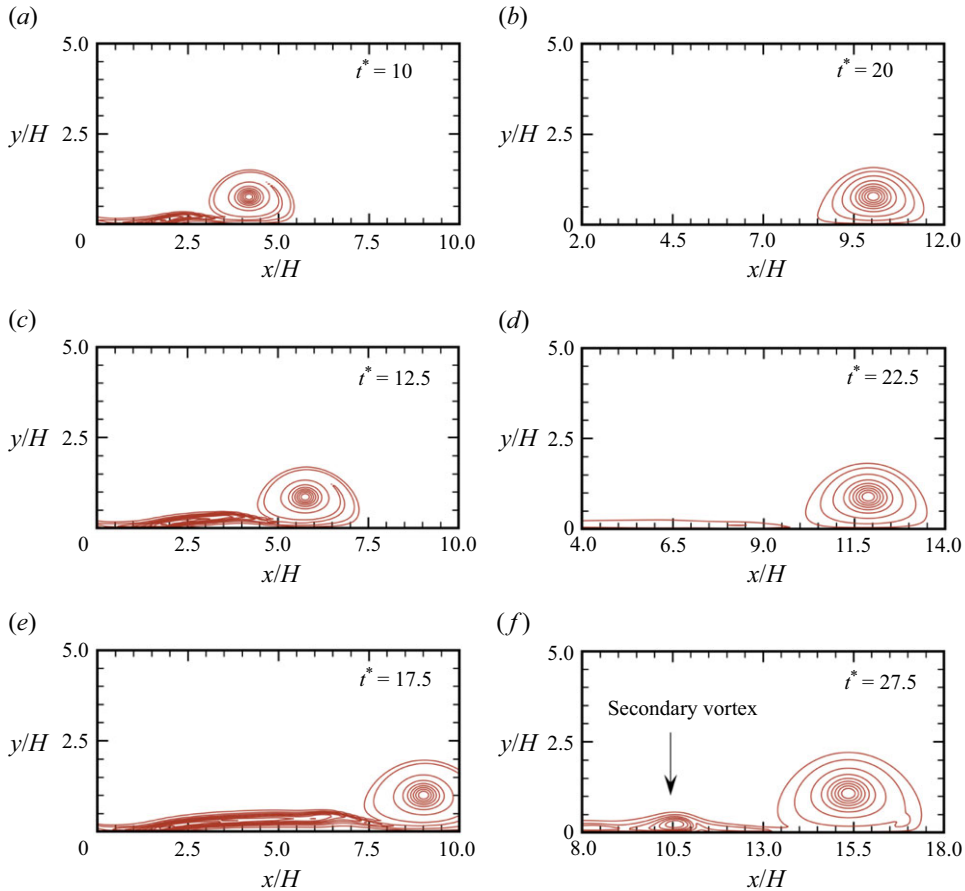


Figure 5. Normalized vorticity fields for the orifice nozzle at stroke ratio of (a,b) 7.5, (c,d) 10 and (e,f) 15. The vorticity field has 10 levels from 0.05 to 1.

*et al.* 1998), a complete pinch-off might require non-dimensional time up to two times the formation number for an axisymmetric jet. A clear pinch-off for vortex pairs before the termination of jet discharge was also not observed in the present studies. Therefore, cases with larger stroke ratio could be meaningful for better understanding of the whole pinch-off process in starting jets. Additionally, a clear pinch-off for vortex dipoles was also not observed by the visualization in the experiment for stroke ratio up to 51 (Afanasyev 2006). This might be due to the low Reynolds numbers (of the order of hundreds). It is also noted that a clear pinch-off also could not be found in axisymmetric jets at low Reynolds numbers even though the vortex ring has attained the maximum circulation level (Bi & Zhu 2020).

The appearance of a trailing jet in the present simulations is different from the initial absence of a trailing jet in the experiments of non-parallel planar starting jets generated by a rectangular nozzle with an aspect ratio of 40 (Steinfurth & Weiss 2020). In their experiments, the leading vortex ring could absorb all vorticity from the nozzle exit up to a formation time of 12. Vortex pinch-off was not observed. This may be due to the initial absence of a trailing jet. The result was explained by the effects of high normalized over-pressure (greater than 1) at the nozzle exit. The present orifice cases are with low normalized over-pressure  $p_{over}^* = (p_{exit} - p_{\infty})/\rho U^2 \approx 0.5$ , where  $p_{exit}$  and  $p_{\infty}$  are the

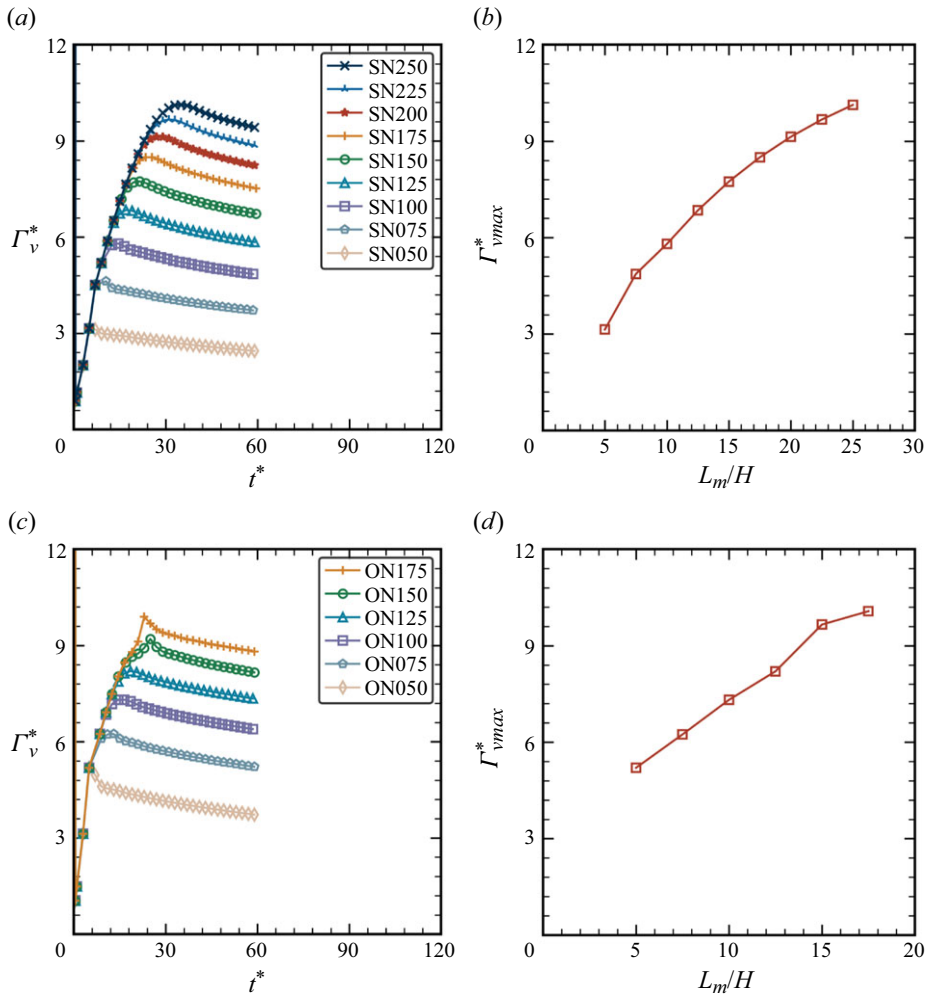


Figure 6. Development of normalized vortex circulation (a,c) and maximum vortex circulation versus stroke ratio (b,d) for straight nozzle (a,b) and orifice nozzle (c,d).

pressure at the nozzle exit centre and the pressure at the ambient fluid. It is noted that the absence of a trailing jet was also not observed in experiments of non-parallel axisymmetric jets with low over-pressure of about 0.4 by Krieg & Mohseni (2013). Therefore, the appearance of a trailing jet and absence of significant vortex growth in the present studies might be due to the low magnitude of over-pressure.

To quantify the growth of the vortex pair, the evolution of vortex circulation is presented in figure 6. Before the trailing pressure maximum appears, the vortex circulation can be approximated by the total circulation. The vortex circulation is normalized as  $\Gamma_v^* = \Gamma_v/UH$ . As shown in figure 6(a,c), the leading vortex pair continuously absorbs vorticity from the trailing jet even after the termination of piston motion. Due to the self-induced velocity, the vortex pair eventually disconnects from the trailing jet and starts its decaying stage. This process also can be found in the formation of the leading vortex ring (Rosenfeld *et al.* 1998). For the orifice cases, the shear layer is more unstable than that for the straight nozzle. Although the Kelvin–Helmholtz instability is not observed during the jet discharge, secondary vortices in the trailing jet appear for cases ON150 and ON175 due to

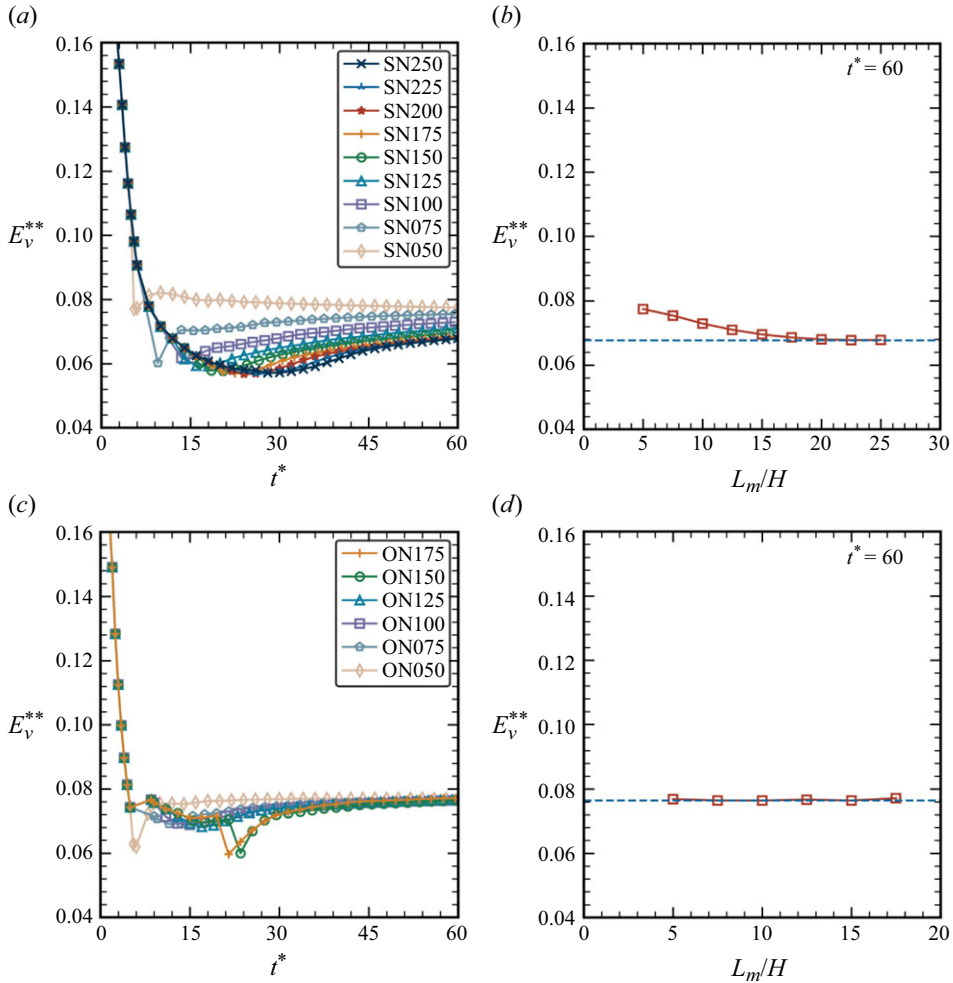


Figure 7. Development of normalized vortex energy (a,c) and vortex energy at  $t^* = 60$  versus stroke ratio (b,d) for straight nozzle (a,b) and orifice nozzle (c,d).

the perturbation caused by the termination of jet discharge (see figure 5f). Thus, the vortex circulation can increase rapidly by vortex pairing.

The maximum vortex circulation for each case is plotted in figure 6(b,d). For straight nozzle cases, the growth rate of vortex circulation becomes smaller with the increase of stroke ratio. This convergent tendency suggests a limiting situation in vortex pair formation, which is analogous to tube-generated vortex ring formation (Gharib *et al.* 1998). For the orifice cases, the increase of slope can be explained by the vortex pairing with the trailing vortex. After the pairing, the leading vortex moves faster due to the increased circulation strength. This process leads to a significant decrease in the growth of vortex circulation after  $L_m/H = 15$ . This result therefore agrees with the trend of the limiting situation in vortex formation analogous to orifice-generated vortex ring formation (Limboung & Nedić 2021c).

To further examine the state of the vortex pair, the evolution of vortex energy is presented in figure 7. The vortex energy is normalized as  $E_v^{**} = E_v / \rho \Gamma_v^2$ . Large and small values of the normalized energy are represented by thin and thick vortex pairs

(Pierrehumbert 1980). As shown in figure 7(a,c), the vortex core develops into a thick core with decreasing non-dimensional energy. The thickest state of a vortex pair is generally enhanced and postponed by the increasing stroke ratio. The vortex pairing process of large-stroke-ratio orifice cases (cases ON150 and ON175) greatly thickens the leading vortex core within a short time. The trailing jet for case ON175 is more energetic on account of the longer jet discharging time, leading to an earlier vortex pairing. During the post-formation stage where the leading vortex becomes stable and decays steadily after a complete pinch-off, vortex pairs generated by non-parallel jets settle to a constant state of energy faster than those of parallel jets. The convergence of vortex energy with respect to a nearly constant vortex impulse after a complete pinch-off from the trailing jet satisfies the suggestion of Kelvin's variational principle. For the energy at  $t^* = 60$ , the vortex energy for straight nozzle cases converges to a universal value of about 0.068 (figure 7b). For the orifice cases, the universal energy is at about 0.076 (figure 7d). The universal energy of steady vortex rings was also observed in experiments (Gharib *et al.* 1998). A thicker straight-nozzle-generated vortex core (i.e. smaller non-dimensional energy) than the orifice-generated vortex core also could be found in starting axisymmetric jets (Rosenfeld, Katija & Dabiri 2009; Krieg & Mohseni 2021). This might be explained by the thicker shear layer of straight nozzle cases and slower vortex motion due to the absence of the over-pressure effect.

On account of the aforementioned similarities between vortex ring formation and vortex pair formation, the formation number (i.e. the onset of pinch-off) will be further studied in two-dimensional flows. Five criteria are presented here, including three local analyses (total circulation, vortex velocity and induced velocity criteria) and two global analyses (entrainment and circulation ratio criteria). The formation numbers will be identified by the circulation criterion first and subsequently they will be further analysed by the other four criteria.

#### 4.1. Circulation criterion

The formation number  $F$  may be determined by the circulation criterion (Gharib *et al.* 1998) when the total circulation  $\Gamma_t^* = \Gamma_t/UH$  becomes equal to the maximum vortex circulation (Rosenfeld *et al.* 1998). In terms of locally maximum vortex circulation  $\Gamma_{vmax}^*$  for each case, the difference between cases SN225 and SN250 is 5% while that for cases ON150 and ON175 is about 4%. The differences are small enough to approximate maximum vortex circulation with errors of about 5% by averaging these two cases (i.e. the two highest values in vortex circulation) for both nozzles. As shown in figure 8, the formation numbers (red arrows) are found by the intersection of total circulation (black solid line) and maximum vortex circulation (blue dashed line). The formation numbers are about 13.6 and 9.3 for the straight nozzle and orifice nozzle, respectively. These are much larger than the 4 and 2 for axisymmetric jets (Gharib *et al.* 1998; Limbourg & Nedić 2021c).

For the non-parallel jet, the formation number of 7 found in Gao & Yu (2016a) is smaller than that found in the present study. The smaller value may be attributed to the trailing jet instability at higher Reynolds number (Zhao *et al.* 2000; Gao & Yu 2012).

#### 4.2. Entrainment criterion

To examine the entrainment property of starting jets, the area of scalar-carrying fluid is shown in figure 9. The area  $A_{sc}^* = A_{sc}/H^2$  is computed inside the jet boundary which is defined above a threshold of 1% for scalar concentration (Sau & Mahesh 2007). The jet area increases linearly for the impulsive piston motion. After the termination of piston

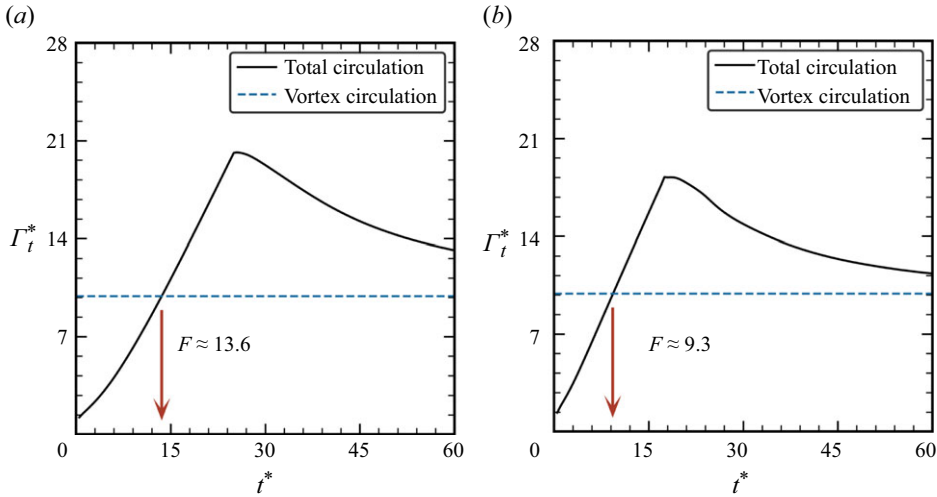


Figure 8. Circulation criterion to determine formation number for (a) straight nozzle (total circulation obtained from case SN250 and vortex circulation obtained from the average of cases SN225 and SN250) and (b) orifice nozzle (total circulation obtained from case ON175 and vortex circulation obtained from the average of cases ON150 and ON175).

motion, the slopes become nearly constant (figure 9a,c). The increase can be attributed to diffusion and mixing of ambient fluids. A constant slope for the rate of area change for  $L_m/H \leq F$  and a decreased slope for  $L_m/H > F$  (Sau & Mahesh 2007) are found. The different growth rates of  $dA_{sc}^*/dt^*$  in terms of stroke ratio can be explained by the fact of the different mixing abilities between the leading vortex and the trailing jet. More and more vorticity would be accumulated in the trailing jet with the increase of stroke ratio for  $L_m/H > F$ . As a consequence, the relative contribution of the leading vortex to the total entrainment decreases as the stroke ratio increases. As shown in figure 9(b,d), the growth rates of  $dA_{sc}^*/dt^*$  decrease significantly after the critical formation time. This situation in two-dimensional flows is similar to the situation in axisymmetric flows (Sau & Mahesh 2007). Based on the intersection of the fitted lines (blue dashed lines), the formation numbers (13.4 for the straight nozzle and 9.6 for the orifice nozzle) can be determined with a prior knowledge of the formation number. The differences between the circulation criterion and the entrainment criterion are about 1 % and 3 % for the straight nozzle and the orifice nozzle, respectively.

### 4.3. Kinematic criterion

A kinematic criterion in terms of the translational velocity was also proposed in previous studies for axisymmetric jets (Mohseni & Gharib 1998; Shusser & Gharib 2000). Pinch-off starts when the vortex ring velocity equals a specific velocity (e.g. the jet velocity near the leading vortex). A specific value  $N$  is defined as the ratio of this particular velocity to the space-averaged velocity at the nozzle exit. This specific value  $N$  in parallel jets is 0.5 from a Hamiltonian theory for vortex rings (Mohseni & Gharib 1998) or about 0.6 from the analytical model with a closure from experimental results (Shusser & Gharib 2000). By the fourth-order central-difference approximation, the vortex velocity can be determined from the vortex trajectory. Moreover, the normalized vortex translational velocity is defined as  $U_v^* = U_v/U$ . Based on the formation numbers found from the circulation criterion, the value  $N$  can be identified to be about 0.49 (figure 10a) and 0.58 (figure 10b) for the straight nozzle and orifice nozzle, respectively. Thus, our results for vortex pair formation

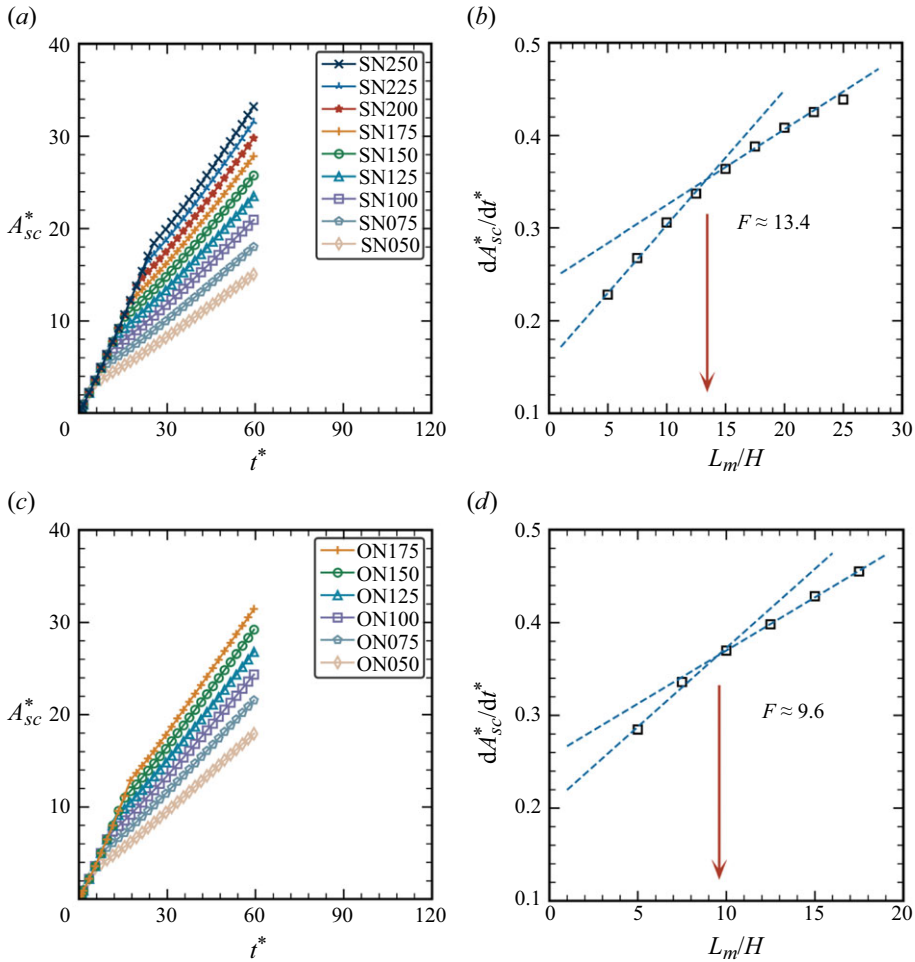


Figure 9. Development of normalized area of scalar-carrying fluid (*a,c*) and normalized growth rate of the area versus stroke ratio (*b,d*) for straight nozzle (*a,b*) and orifice nozzle (*c,d*).

can generally agree with the suggestions (Mohseni & Gharib 1998; Shusser & Gharib 2000) and measurements (Limbourg & Nedić 2021*d*) for axisymmetric flows.

Recently, another kinematic criterion was proposed for axisymmetric jets (Krieg & Mohseni 2021). Pinch-off starts when the characteristic vortex velocity reaches a characteristic feeding velocity of  $2U$ . The characteristic vortex velocity is also commonly referred to as the induced velocity  $U_{cmax}^*$  ( $= U_{cmax}/U$ ). Velocity  $U_{cmax}^*$  is the maximum velocity along the centreline. The streamwise location of the induced velocity is determined by the streamwise trajectory of the vortex pair. Based on the formation numbers obtained from the circulation criterion, the induced velocity criteria are found to be about  $1.75U$  and  $2.12U$  for the straight nozzle (figure 11*a*) and orifice nozzle (figure 11*b*), respectively.

#### 4.4. Maximum circulation criterion

The ratio of the maximum vortex circulation to maximum total circulation  $\Gamma_{vmax}^*/\Gamma_{tmax}^*$  is defined to examine the efficiency of starting jets on vortex formation. The ratio decreases as the stroke ratio increases due largely to the existence of the trailing jet from small

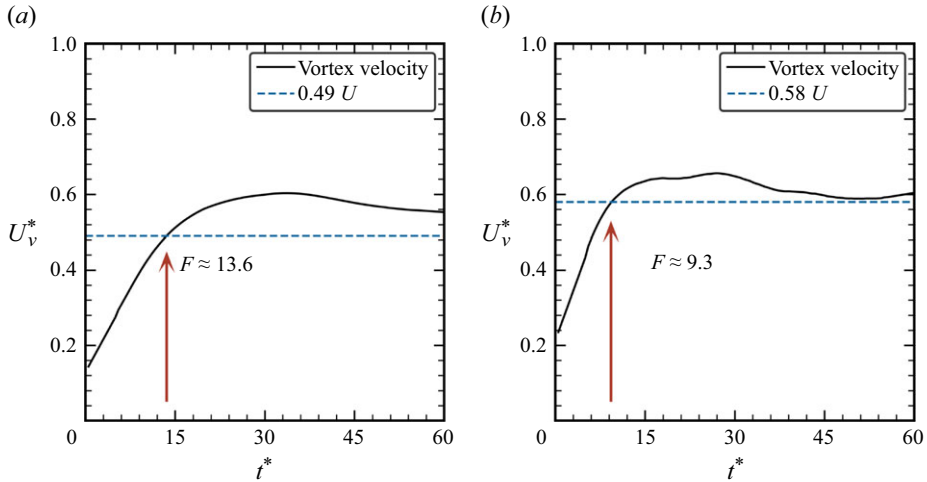


Figure 10. Development of vortex translational velocity for (a) straight nozzle (case SN250) and (b) orifice nozzle (case ON175).

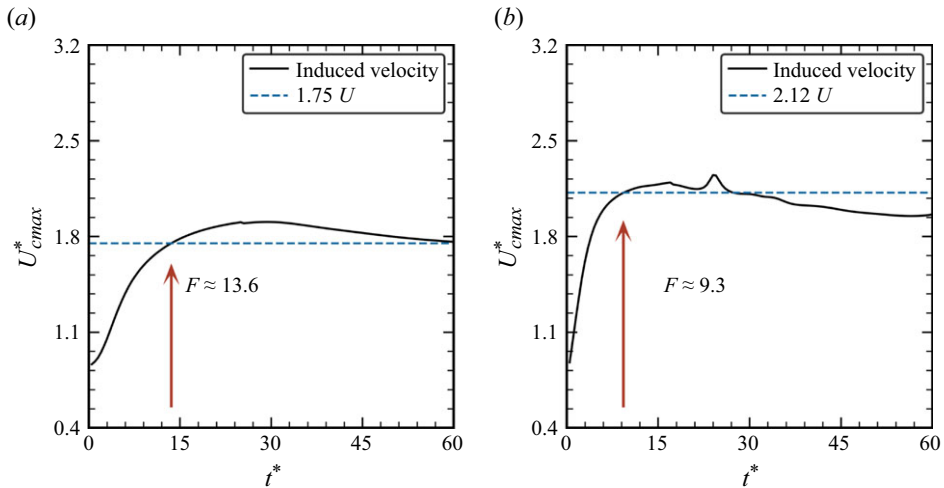


Figure 11. Development of induced velocity for (a) straight nozzle (case SN250) and (b) orifice nozzle (case ON175).

formation time (such as  $t^* = 1$ ). Based on the formation time obtained from the circulation criterion, the circulation ratio criterion is defined when the ratio reaches a critical value. A universal ratio of about 72 % is found to be appropriate for both nozzle configurations in two-dimensional flows (see figure 12). Therefore, this criterion is not similar to the kinematic criterion due to its independence of the nozzle configuration. The formation number represents a critical circulation ratio for vortex formation in starting jets. This criterion agrees well with the experiment for non-parallel two-dimensional starting jets with a critical ratio of about 71 % (Gao & Yu 2016a).

Considering the contraction effect, the transformed formation number has been used to unify the classical formation number for the straight nozzle and orifice nozzle (Limbourg

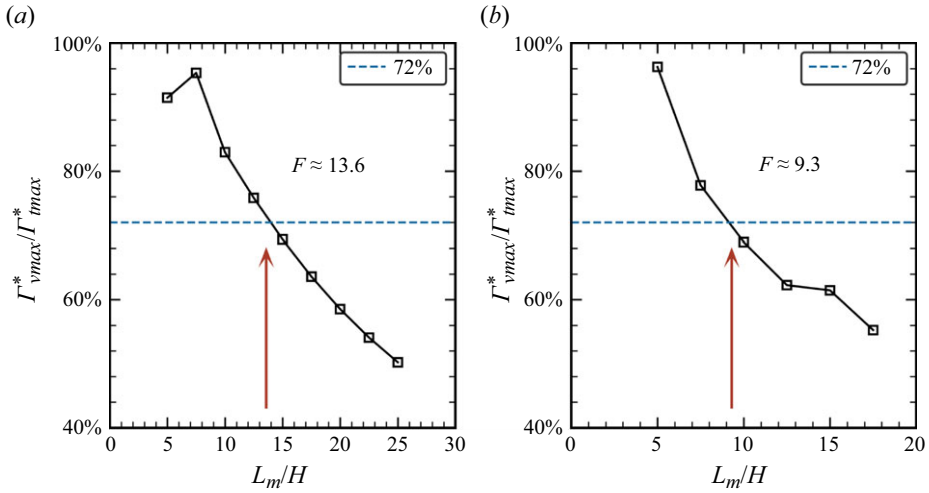


Figure 12. Circulation ratio versus stroke ratio for (a) straight nozzle and (b) orifice nozzle.

& Nedić 2021b), such as

$$F_{\star} = \frac{U_{\star} t_{critical}}{H_{\star}} = \frac{U t_{critical}}{H} \times 1/C_c^2 = F \times 1/C_c^2, \tag{4.1}$$

where the contraction coefficient  $C_c$  is 0.9 suggested for the straight nozzle (Limbourg & Nedić 2021b) or 0.76 for the orifice nozzle. The contraction coefficient  $C_c$  is obtained from the steady simulation and identified from the lowest transversal position along the streamline passing the inner corner of the orifice plate. Quantity  $t_{critical}$  is the physical time corresponding to the critical formation time. Based on (4.1), the present formation numbers of 13.6 and 9.3 ( $F$ ) will become 16.8 and 16.1 ( $F_{\star}$ ) for the straight nozzle and orifice nozzle, respectively. Therefore, the transformed formation number ( $F_{\star}$ ) of 16.5 with deviation  $\pm 0.4$  can effectively unify the critical formation time for the straight nozzle case and orifice case. In additional, with the use of the contraction coefficient, two kinematics criteria also can be universal for both nozzle configurations. For the first kinematic criterion (§ 4.3), the critical translational velocity of about  $0.44U_{\star}$  is universal for the straight nozzle and orifice nozzle. This conclusion agrees well with the experiments for axisymmetric jets (Limbourg & Nedić 2021d). For the second kinematic criterion (§ 4.3), the critical induced velocity of about  $1.60U_{\star}$  is also found to be nearly independent of the nozzle configuration. The deviations for both straight nozzle and orifice nozzle are within  $0.03U_{\star}$ .

#### 4.5. Effects of Reynolds number

Some studies indicated that the development of vortex circulation (i.e. the formation number and the scaling law for axial and radial trajectories) is nearly independent of the Reynolds number for laminar vortex rings (Didden 1979; Gharib *et al.* 1998). The insignificant influence on the formation number of laminar vortex rings has been examined by a series of simulations over a range of Reynolds numbers from 500 to 5000. It is noted that the Reynolds number would play an important role to the velocity profile at the nozzle exit plane (Rosenfeld *et al.* 1998, 2009). To evaluate the dependence of formation number on the Reynolds number, several more cases are simulated as listed in table 3. To avoid any possible developments of transitional or turbulent flows, the Reynolds numbers are

Case	$\Delta x = \overline{\Delta y}$	$Re_H$	$\Gamma_{tmax}^*$	$\Gamma_{vmax}^*$	$F$
SN250-Re500	$H/100$	500	21.0	9.6	12.0
SN250	$H/100$	1000	20.2	10.1	13.8
SN250-Re1600	$H/180$	1600	19.1	10.1	14.7
SN250-Re2000	$H/180$	2000	18.5	9.7	14.7
ON175-Re500	$H/100$	500	16.4	8.8	9.1
ON175	$H/100$	1000	18.2	10.1	9.5
ON175-Re1600	$H/180$	1600	19.3	8.5	7.7
ON175-re2000	$H/180$	2000	19.6	7.6	6.8

Table 3. Cases studied for the dependence of the formation number on the Reynolds number.

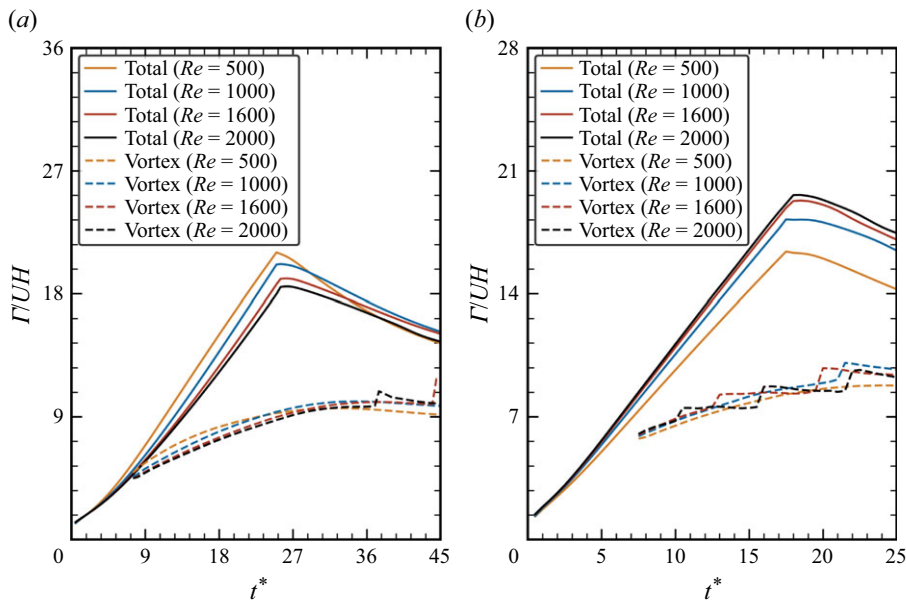


Figure 13. Effects of the Reynolds number on the evolution of total circulation and vortex circulation for (a) straight nozzle and (b) orifice nozzle.

chosen up to 2000. Due to more shear-layer instabilities for higher Reynolds numbers (e.g. 1600 and 2000), finer meshes with an average grid spacing of  $H/180$  in streamwise and transverse directions are used to provide more precise results for the straight nozzle and the orifice nozzle. The evolutions of total circulation and vortex circulation are presented in figure 13. According to the circulation criterion, the formation numbers are identified for different Reynolds numbers, as summarized in table 3.

As can be seen in figure 13(a), the total circulation generated by the straight nozzle would be larger for smaller Reynolds number (Rosenfeld *et al.* 1998). This can be attributed to the viscous effect which produces a thicker boundary layer within the nozzle with higher vorticity. Similar reason contributes to higher vortex circulation initially. However, the vortex circulation for case SN250-Re500 gradually becomes smaller than that for other cases with the straight nozzle due to the viscous diffusion. The greater total circulation and smaller maximum vortex circulation for case SN250-Re500 bring down the formation number slightly to 12. As indicated by table 3, the maximum vortex circulation is identical

for cases SN250 and SN250-Re1600. Therefore, the influence of Reynolds number on the local maximum of vortex circulation is limited. However, the formation number for case SN250 is smaller due to larger total circulation increase rate. The final increase of vortex circulation generated by the vortex pairing with the secondary vortex appearing after the jet discharge is excluded to identify the formation number for cases SN250-Re1600 and SN250-Re2000. This is because the local maximum of vortex circulation has already been achieved. This phenomenon is different from that of the non-parallel flow cases which still have a continuous increase of vortex circulation before the vortex pairing. The difference may be explained by the stronger shear-layer instability for orifice cases. Stronger secondary vortex for case SN250-Re2000 contributes to a faster pinch-off and smaller vortex circulation in comparison with case SN250-Re1600. However, due to the smaller total circulation increase rate, the formation number for case SN250-Re2000 is maintained. It is noted that the formation number could be increased slightly with the Reynolds number for the straight nozzle due to a decrease in total circulation. In comparison with the formation number of 13.6 for the straight nozzle, the differences produced by the Reynolds numbers from 500 to 2000 are within 12%. This range agrees well with the comparable difference of about 10% in experiments and simulations for axisymmetric jets (Gharib *et al.* 1998; Rosenfeld *et al.* 1998).

Different from the situation for the straight nozzle, the total circulation for the orifice cases could be enhanced with the increasing Reynolds number due to greater transverse velocity gradient at higher Reynolds numbers (see [figure 13b](#)). The increase of vortex circulation becomes smaller as the Reynolds number increases. This leads to similar vortex circulation for cases ON175, ON175-Re1600 and ON175-Re2000 initially and smaller vortex circulation for case ON175-Re500. Therefore, the formation number for case ON175-Re500 is smaller than that at Reynolds number of 1000. Higher Reynolds number induces more shear-layer instabilities (e.g. double vortex pairing for case ON175-Re1600 and triple vortex pairing for case ON175-Re2000). This leads to a faster pinch-off and smaller formation number identified by the local maximum vortex circulation during a constant state after the first vortex pairing. The onset of pinch-off can appear earlier by up to 27% (in comparison with the formation number of 9.3) due to the appearance of secondary vortices in the trailing jet. This result agrees well with previous findings in simulations for axisymmetric jets (Zhao *et al.* 2000). Additionally, the formation numbers for cases ON175-Re1600 and ON175-Re2000 also agree with the range found by earlier experiments with the orifice nozzle and Reynolds numbers from 1490 to 3380 (Gao & Yu 2016a).

## 5. Two-dimensional flows versus axisymmetric flows

After determining the range of formation numbers in the preceding sections, we focus on the difference in the formation number between the axisymmetric and two-dimensional cases. Slower vortex motion in two-dimensional flows has been attributed to be the reason (Pedrizzetti 2010; Domenichini 2011). For more quantitative discussions on the differences between axisymmetric and two-dimensional flows, two axisymmetric cases (case ASN100 for the straight nozzle and case AON100 for the orifice nozzle) with stroke ratio  $L_m/D = 10$  are further simulated for comparisons. As shown in [figure 14](#), the translational velocity of the vortex rings is far greater than the translational velocity of the vortex pairs, as may have been expected. The oscillation of vortex velocity may be attributed to the vorticity redistribution during the pinch-off process and the non-circular geometry of the vortex core at the post-formation process (Danaila & Helie 2008). To examine the factors influencing the translational velocity, the self-induced velocity of a

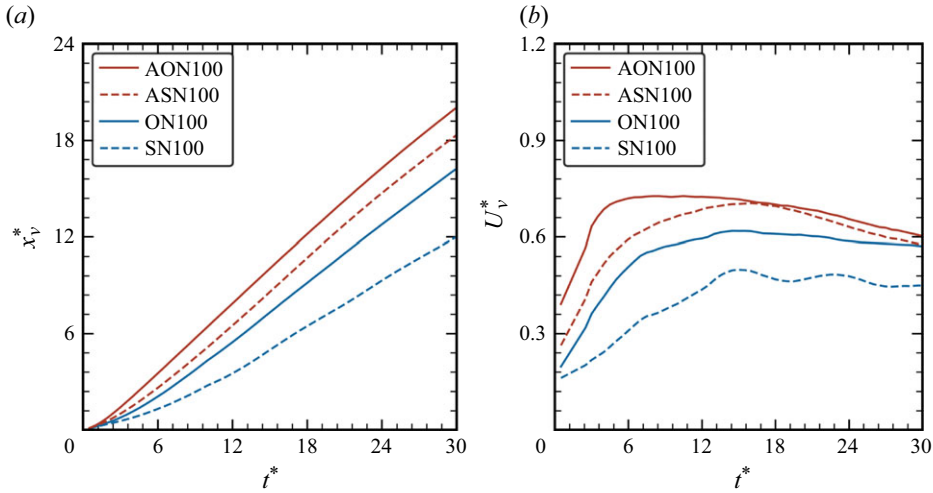


Figure 14. Development of (a) normalized streamwise trajectory and (b) normalized translational velocity of the leading vortex.

curved vortex filament can be estimated by the Biot–Savart law (Lim & Nickels 1995):

$$\mathbf{u} = \frac{\Gamma\kappa}{4\pi} \ln\left(\frac{R_c}{a}\right) \mathbf{b}, \tag{5.1}$$

where  $\kappa$  is the local curvature;  $R_c$  is the radius of curvature;  $a$  is the radius of the vortex core; and  $\mathbf{b}$  is the unit vector along the binormal direction. At the initial formation time ( $t^* < 1$ ), the vortex core is small enough to provide a constant term  $\ln(R_c/a)$  (Wu, Ma & Zhou 2007). The vortex circulation may be evaluated by the total circulation in the initial formation. Based on the numerical results, the vortex pair would have larger circulation but smaller translational velocity during the initial formation in comparison with the vortex ring. This result suggests that the local curvature is more important than the vortex circulation in estimating vortex translational velocity even though they are of the same order in the Biot–Savart law.

The velocity formula for the steady vortex can be used to further understand the faster motion of vortex rings. For two-dimensional flows, the translational velocity of a vortex pair considered as two point vortices can be expressed by (Saffman 1992)

$$U_v = \frac{\Gamma_v}{4\pi y_v}. \tag{5.2}$$

For axisymmetric flows, the vortex ring velocity depends on its core thickness when the curvature of the vortex tube is considered. The translational velocity of a thin-cored vortex ring can be expressed by a second-order formula as (Fraenkel 1972)

$$U_v = \frac{\Gamma_v}{4\pi y_v} \underbrace{\left\{ \ln\left(\frac{8}{\varepsilon}\right) - \frac{1}{4} + \varepsilon^2 \left[ \frac{15}{32} - \frac{3}{8} \ln\left(\frac{8}{\varepsilon}\right) \right] \right\}}_I, \tag{5.3}$$

where mean core radius  $\varepsilon$  is defined as the ratio of the core radius  $a$  to ring radius  $y_v$ . A universal energy of a steady thin vortex ring was found to be 0.33 (Gharib *et al.* 1998; Limbourg & Nedić 2021c), leading to a specific ratio  $\varepsilon$  of about 0.5 in the family of steady vortex rings (Norbury 1973). Thus, the term  $I$  in equation (5.3) represents the effect of core size and is equal to approximately 2.4. Based on the results of vortex circulation

$t^*$	Case	Geometry	$\Gamma_v^*$	$y_v^*$	$U_v^*$
12	SN100	Straight nozzle	5.74	0.87	0.53
12	ON100	Orifice nozzle	7.12	0.86	0.66
12	ASN100	Straight nozzle	3.64	0.87	0.80
12	AON100	Orifice nozzle	3.37	0.91	0.71
30	SN100	Straight nozzle	5.33	0.87	0.49
30	ON100	Orifice nozzle	6.89	0.91	0.60
30	ASN100	Straight nozzle	2.96	1.01	0.56
30	AON100	Orifice nozzle	3.08	1.06	0.56

Table 4. Estimated translational velocity using equations (5.2) and (5.3).

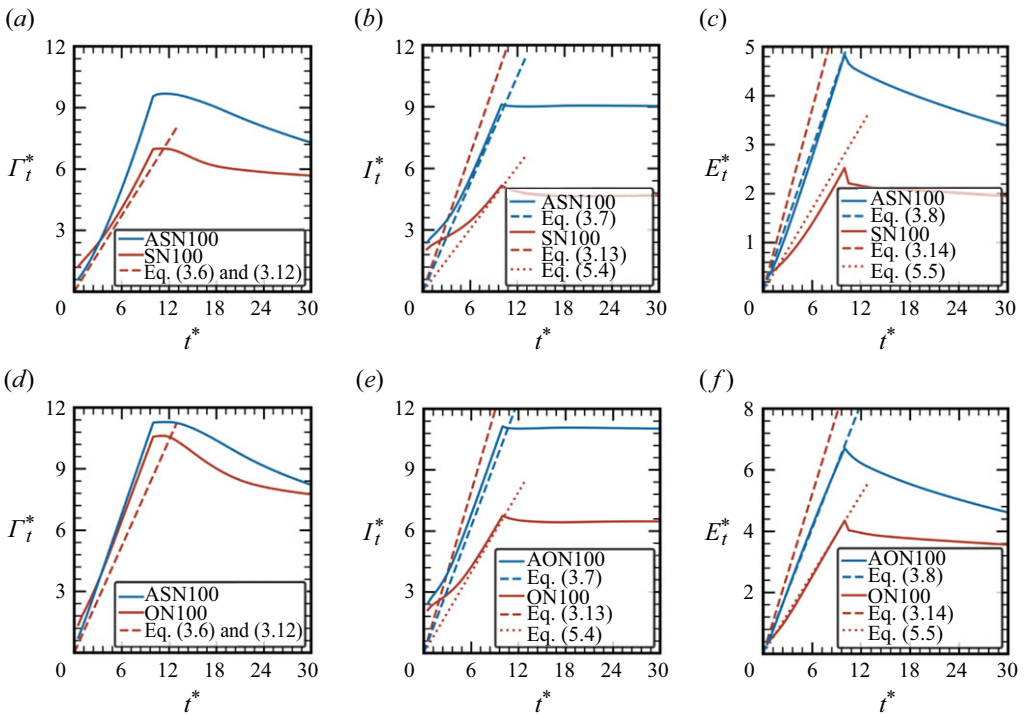


Figure 15. Evolution of normalized total invariants: (a,d) circulation, (b,e) impulse and (c,f) energy for straight nozzle (a–c) and orifice nozzle (d–f).

and transverse trajectory, the velocities at  $t^* = 12$  and  $t^* = 30$  are calculated for vortex pairs and vortex rings as listed in table 4. The magnitude of the calculated velocity at both instants approximately agrees with the translational velocity obtained from numerical results (figure 14b). At  $t^* = 12$ , the circulation is larger for vortex pairs than for vortex rings while the difference in transverse trajectory is negligible. However, the velocity of the vortex ring is larger. This suggests the important effect of the local curvature.

As expected, total invariants are different between axisymmetric flows and two-dimensional flows. They are reflected in the velocity distribution over the nozzle exit. This influence on total invariants and the accuracy of the contraction-based slug model

(equations (3.6)–(3.8) for axisymmetric flows and equations (3.12)–(3.14) for two-dimensional flows) are evaluated in figure 15. The contraction coefficient  $C_c$  for the axisymmetric flow is found to be 0.73 from the steady simulation. Therefore, the difference of  $C_c$  for the two-dimensional flow and axisymmetric flow is negligible, in accord with previous discussions (Limbourg & Nedić 2021a,b). Here, the results for the axisymmetric flow are approximately predicted by the two-dimensional  $C_c$ .

First, an evaluation of circulation prediction is conducted. It is noted that the formulas of circulation prediction are identical for two-dimensional and axisymmetric flows (equations (3.6) and (3.12)). As can be seen in figure 15(a,d), the contraction-based slug model can approximately predict the total circulation of axisymmetric flows at small time (e.g.  $t^* < 4$ ). A better estimation than that of the classical slug model (corresponding to a smaller slope of invariant growth) can be observed as in a previous study (Limbourg & Nedić 2021a). However, the development of boundary-layer thickness brings increasing deviation between the numerical result and the contraction-based model. Due to a reduction of boundary-layer thickness, the contraction-based model can appropriately predict total circulation in two-dimensional flows. The relative error for the prediction of the straight nozzle case at  $t^* = 10$  (which is the end of the piston motion and is around the critical formation time) is  $-11\%$ . In addition, the contraction-based slug model can also provide approximate predictions for orifice cases in both two-dimensional and axisymmetric flows. The relative error for the two-dimensional prediction of the orifice case at  $t^* = 10$  is  $-18\%$ .

For the prediction of total impulse  $I_t^* = I_t/\rho D^3 U$  and total energy  $E_t^* = E_t/\rho D^3 U^2$  for axisymmetric flows, the contraction-based slug model (blue dashed lines in figure 15) can generally provide accurate descriptions. Although the initial over-pressure effect on total impulse cannot be included, the error for prediction is insignificant at later time (e.g.  $t^* > 6$ ). However, due to the two-dimensional nature, the contraction-based slug model for two-dimensional flows (red dashed lines) predicts larger slopes than that of axisymmetric flows for total impulse  $I_t^* = I_t/\rho H^2 U$  and total energy  $E_t^* = E_t/\rho H^2 U^2$ . This overestimated behaviour of the slug model is not found in two-dimensional flows. In reality, the total momentum and total energy are lower for two-dimensional flows due to slower vortex motion. In comparison with the difference in total circulation between two-dimensional and axisymmetric flows, larger differences can be observed for total impulse and total energy. This can be attributed to the two-dimensional characteristic for circulation and the three-dimensional characteristic for impulse and energy in axisymmetric flows.

To improve the contraction-based slug model for two-dimensional flows, a modified coefficient  $C_m$  is proposed for impulse and energy formulas. Equations (3.13) and (3.14) are rewritten as

$$I_{*2m} = \rho L H U \times 1/C_c \times 1/C_m, \quad (5.4)$$

$$E_{*2m} = \frac{1}{2} \rho L H U^2 \times 1/C_c^2 \times 1/C_m, \quad (5.5)$$

where the modified coefficients are 2.2 and 2.0 for the straight nozzle and orifice nozzle, respectively. As shown in figure 15, the modified contraction-based slug model for two-dimensional flows (red dotted lines) can appropriately predict the total impulse and total energy. The relative errors of the total invariants predicted by the modified contraction-based slug model (equations (3.12), (5.4) and (5.5)) can be found in table 5. Errors are obtained by time averaging between  $t^* = 5$  and  $t^* = 10$ .

Dimension	Geometry	$\Gamma_t^*$	$I_t^*$	$E_t^*$
Two-dimensional	Straight nozzle	-10 %	-7 %	18 %
Two-dimensional	Orifice nozzle	-19 %	-5 %	2 %

Table 5. Time-averaged relative errors for the modified contraction-based slug model.

### 6. Analytical estimation of two-dimensional formation number

For axisymmetric flows, an asymptotic matching procedure was proposed to analytically estimate the formation number. The total invariants described by the slug model were matched to a model of steadily isolated vortex rings such as the Norbury–Fraenkel model (Norbury 1973) or Kaplanski–Rudi model (Kaplanski & Rudi 2005). Ultimately, the critical time scale was obtained by an additional closure assumption, for example, a universal vortex energy in non-dimensional form (Gharib *et al.* 1998), a specific vortex velocity normalized by the initial jet velocity (Mohseni & Gharib 1998; Shusser & Gharib 2000) or a volume constraint of vortex ring bubble (Linden & Turner 2001). In addition, the contraction-based slug model was used to predict the formation number (Limbourg & Nedić 2021*d*).

For two-dimensional flows, a family of steady vortex pairs (Pierrehumbert 1980) may be used to further predict the formation number. To the best of the authors’ knowledge, the asymptotic matching procedure has not been studied for two-dimensional starting jets. A parameter  $\bar{A}_0 = A_0/A_1$  was typically used to identify the member in the Pierrehumbert model, where  $A_0$  is the minimum distance of the core boundary from the symmetry axis and  $A_1$  is the maximum distance from the symmetry axis. However, distance  $A_0$  only can be identified when the leading vortex pair moves far away from the trailing jet. This is owing to the influence of the trailing jet during jet discharge from the nozzle. Instead, another geometrical parameter  $\gamma = y_v/A_1$  can be used to determine the vortex member in the current study. As shown in figure 16(a), vortex pairs generated by various nozzle configurations and stroke ratios eventually reach a universal value at  $\gamma = 0.49$  (averaged from all cases). This result generally agrees with the conclusion from figure 7 and the suggestion of a universal vortex ring generated by various starting jets (Gharib *et al.* 1998).

The Pierrehumbert model provides a one-to-one correspondence between the geometrical parameter  $\gamma$  and the non-dimensional vortex energy  $E_v^{**}$  (square symbols in figure 16b). The relation may be approximated by a quartic polynomial (blue dotted line) as

$$E_v^{**} = 10.875\gamma^4 - 26.434\gamma^3 + 24.032\gamma^2 - 8.898\gamma + 1.186. \tag{6.1}$$

It is noted that the Pierrehumbert vortex with  $\gamma = 0.49$  and  $E_v^{**} = 0.11$  has overestimated the non-dimensional vortex energy of the simulated vortex pairs with differences of 62 % and 45 % for the straight nozzle and orifice nozzle, respectively.

Combining the proposed slug model (equations (3.12), (5.4) and (5.5)) and the definition of vortex energy normalization ( $E_v^{**} = E_v/\rho\Gamma_v^2$ ), the relation between stroke ratio and vortex energy can be represented as

$$\frac{L}{H} = \frac{2C_c^2}{C_m E_v^{**}}. \tag{6.2}$$

The required stroke ratio to generate a particular vortex pair can be estimated from (6.1) and (6.2). The limiting cases of vortex pairs are a thick axis-touching vortex for  $\gamma \rightarrow 0.413$  and a thin vortex for  $\gamma \rightarrow 1$ . For the limiting cases at  $\gamma \rightarrow 0.413$ , the limiting stroke ratio

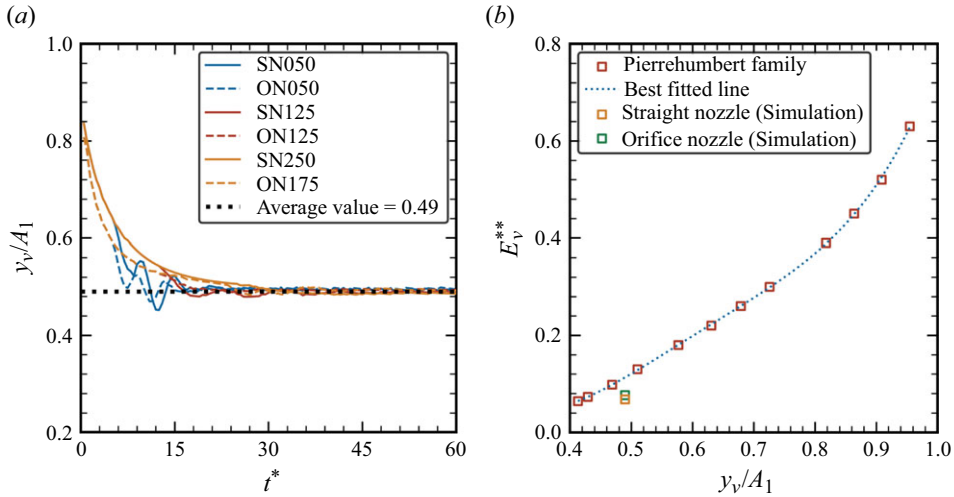


Figure 16. (a) Evolution of parameter  $y_v/A_1$  and (b) comparison of simulated vortices with those from the Pierrehumbert family.

should be at about 11.5 for the straight nozzle and 9.0 for the orifice nozzle. These results suggest the minimum stroke ratio to generate the theoretically thickest vortex pair.

To estimate the formation number, an additional assumption is required. The pinch-off would start when the vortex pair becomes steady. Two models on the basis of this assumption are proposed in terms of the vortex impulse and vortex velocity.

First, an impulse-based model to predict the onset of pinch-off is proposed based on momentum conservation and the assumption of the steady state of a vortex pair. The vortex impulse (Batchelor 1967) can be expressed as

$$I_v = \rho y_v \Gamma_v. \tag{6.3}$$

When the vortex pair is assumed to be bounded in a circular vortex bubble moving with velocity  $U_v$ , the vortex impulse can be approximately expressed as

$$I_v = \rho \pi A_1^2 U_v. \tag{6.4}$$

Combining equations (5.2), (6.3) and (6.4) yields

$$\frac{y_v^2}{A_1^2} = \frac{1}{4}. \tag{6.5}$$

Therefore, a critical geometrical parameter  $\gamma = 0.5$  can be obtained from the impulse-based model for a steady vortex pair. This result agrees with the numerical results shown in figure 16(a). Based on equation (6.1), the critical value of vortex energy is at about 0.12. Inserting this result into equation (6.2) produces critical stroke ratios of 6.1 and 4.8 for the straight nozzle and orifice nozzle, respectively. Although the matching process of vortex impulse allows a prediction of the geometrical parameter, the predictions of the formation numbers are far away from the numerical results due to the error of the Pierrehumbert model in terms of the vortex energy.

Second, the velocity-based model proposes the onset of pinch-off when the vortex velocity reaches the jet velocity near the vortex rear boundary (Shusser & Gharib 2000). With the assumption of jet half-width equalling the transverse trajectory of the vortex pair,

Geometry	Impulse model	Velocity model	Formation number (simulation)
Straight nozzle	6.1 (−55 %)	10.2 (−25 %)	13.6
Orifice nozzle	4.8 (−48 %)	7.3 (−22 %)	9.3

Table 6. Relative errors for analytical models.

the momentum conservation of jet flows allows

$$HU = 2y_v U_v. \tag{6.6}$$

Combining equations (3.12), (5.4) and (6.3) yields

$$y_v = \frac{2C_c H}{C_m}. \tag{6.7}$$

Substituting equation (6.7) into equation (6.6) yields

$$U_v = \frac{C_m U}{4C_c}. \tag{6.8}$$

Combining equations (3.12), (5.2) and (6.7) yields

$$U_v = \frac{C_m L U}{16\pi C_c^3 H}. \tag{6.9}$$

Combining equations (6.8) and (6.9) yields

$$\frac{L}{H} = 4\pi C_c^2. \tag{6.10}$$

Therefore, critical stroke ratios of 10.2 and 7.3 are found for the straight nozzle and orifice nozzle, respectively. The relative errors of formation number prediction are presented in table 6. In comparison with the dynamical model in terms of the vortex impulse, the kinematic model would be more appropriate to predict the formation numbers and reduce the errors by half.

### 7. Concluding remarks

Numerical studies on two-dimensional impulsively starting jets have been conducted to examine the formation of laminar vortex pairs. The main objective of the current work is to explore the universal formation number and corresponding estimation by respective analytical models.

Based on the pressure-based method, the vortex boundary can be identified before a complete pinch-off from the trailing jet. More information on the vortex invariants can therefore be quantified. The local maximum of vortex circulation converges to a maximum with the increase of stroke ratio, suggesting a limiting formation of vortex pairs. Kelvin’s variational principle is satisfied after a complete pinch-off which appears after the termination of the piston motion. The vortex energy increases gradually and finally reaches a limiting value.

Two-dimensional formation numbers (13.6 and 9.3) for the straight nozzle and orifice nozzle are analysed by five criteria including three local analyses (total circulation, vortex velocity and induced velocity criteria) and two global analyses (entrainment and circulation ratio criteria). Typical formation numbers can be transformed into a universal value of about 16.5 for both nozzles by the consideration of contraction for non-parallel

jets. The influence on the formation number is examined over a range of Reynolds numbers from 500 to 2000. In comparison with the formation number of 13.6 for the straight nozzle, differences due to the Reynolds numbers from 500 to 2000 are within 12 %. For the orifice cases, the formation number can generally be reduced up to 27 % by the increase of Reynolds number due to the appearance of trailing shear-layer instability.

Comparing the self-induced velocity of a vortex pair with that of a vortex ring, the curvature significantly accelerates axisymmetric vortex motion and contributes more influence than the circulation. As a result, slower vortex movement can be found in two-dimensional flows and therefore it will augment the formation number in comparison with axisymmetric flows. Slower vortex pairs resist the development of the boundary layer inside the nozzle, leading to a reduction of total circulation for the straight nozzle. Therefore, the contraction-based slug model appropriately predicts the total circulation of the straight nozzle for two-dimensional flows but fails for axisymmetric flows at a later time. The contraction-based slug model can approximately predict the total circulation of the orifice for both two-dimensional and axisymmetric flows. To remedy the limitation of the contraction-based slug model in total impulse and total energy predictions, a modification on two-dimensional flows is proposed and the results are found to perform properly with maximum errors less than 20 %.

Analytical estimation of two-dimensional formation number is conducted by matching total invariants predicted by the proposed slug model to the Pierrehumbert model of steady isolated vortex pairs. On the basis of an assumption of steady vortex motion, two analytical models are proposed in terms of the vortex impulse and vortex velocity. Although the impulse-based model performs worst for the formation number prediction due to the limitation of the Pierrehumbert model, it could accurately predict the universal geometrical parameter of a steady vortex pair produced by starting flows. In comparison with the impulse-based model, the kinematic model could provide appropriate estimations and significantly reduce the errors to about –25 %.

This study identifies the existence of pinch-off in laminar flows and proposes analytical estimations for the universal formation number in two-dimensional vortex formation. More instability effects at a high Reynolds number possibly have a marked influence on the pinch-off process. Further numerical and experimental studies could better address the problem and are therefore suggested here.

**Funding.** Financial support from the Hong Kong Polytechnic University in the form of a postgraduate scholarship for the first author is gratefully acknowledged. This work was also supported by the project from the Science and Technology Department of Sichuan Province (Grant No. 2023YFH0084).

**Declaration of interests.** The authors report no conflict of interest.

#### REFERENCES

- AFANASYEV, Y.D. 2006 Formation of vortex dipoles. *Phys. Fluids* **18** (3), 037103.
- AI, J.J., YU, S.C.M., LAW, A.W.K. & CHUA, L.P. 2005 Vortex dynamics in starting square water jets. *Phys. Fluids* **17** (1), 014106.
- ALLEN, J.J. & NAITOH, T. 2005 Experimental study of the production of vortex rings using a variable diameter orifice. *Phys. Fluids* **17** (6), 061701.
- ARNOLD, V.I. 1965 Conditions for nonlinear stability of stationary plane curvilinear flows of an ideal fluid. *Sov. Math. Dokl.* **162**, 773–777.
- BASKARAN, M. & MULLENERS, K. 2022 Lagrangian analysis of bio-inspired vortex ring formation. *Flow* **2**, E16.
- BATCHELOR, G.K. 1967 *An Introduction to Fluid Dynamics*. Cambridge University Press.
- BENJAMIN, T.B. 1976 The alliance of practical and analytical insights into the nonlinear problems of fluid mechanics. In *Lecture Notes in Mathematics*, vol. 503, pp. 8–29. Springer.

- BI, X. & ZHU, Q. 2020 Pulsed-jet propulsion via shape deformation of an axisymmetric swimmer. *Phys. Fluids* **32** (8), 081902.
- DABIRI, J.O. & GHARIB, M. 2004 Delay of vortex ring pinchoff by an imposed bulk counterflow. *Phys. Fluids* **16** (4), L28–L30.
- DANAÏLA, I. & HELIE, J. 2008 Numerical simulation of the postformation evolution of a laminar vortex ring. *Phys. Fluids* **20** (7), 073602.
- DIDDEN, N. 1979 On the formation of vortex rings: rolling-up and production of circulation. *J. Appl. Math. Phys.* **30** (1), 101–116.
- DOMENICHINI, F. 2011 Three-dimensional impulsive vortex formation from slender orifices. *J. Fluid Mech.* **666**, 506–520.
- FERNÁNDEZ, J.J.P. & SESTERHENN, J. 2017 Compressible starting jet: pinch-off and vortex ring–trailing jet interaction. *J. Fluid Mech.* **817**, 560–589.
- FERNANDO, J.N. & RIVAL, D.E. 2016 Reynolds-number scaling of vortex pinch-off on low-aspect-ratio propulsors. *J. Fluid Mech.* **799**, R3.
- FLIERL, G.R. & MORRISON, P.J. 2011 Hamiltonian–Dirac simulated annealing: application to the calculation of vortex states. *Phys. D: Nonlinear Phenom.* **240** (2), 212–232.
- FRAENKEL, L.E. 1972 Examples of steady vortex rings of small cross-section in an ideal fluid. *J. Fluid Mech.* **51** (1), 119–135.
- GAO, L. & YU, S.C.M. 2012 Development of the trailing shear layer in a starting jet during pinch-off. *J. Fluid Mech.* **700**, 382–405.
- GAO, L. & YU, S.C.M. 2016a Formation of leading vortex pair in two-dimensional starting jets. *AIAA J.* **54** (4), 1364–1369.
- GAO, L. & YU, S.C.M. 2016b Vortex ring formation in starting forced plumes with negative and positive buoyancy. *Phys. Fluids* **28** (11), 113601.
- GAO, L., YU, S.C.M., AI, J.J. & LAW, A.W.K. 2008 Circulation and energy of the leading vortex ring in a gravity-driven starting jet. *Phys. Fluids* **20** (9), 093604.
- GHARIB, M., RAMBOD, E. & SHARIFF, K. 1998 A universal time scale for vortex ring formation. *J. Fluid Mech.* **360**, 121–140.
- KAPLANSKI, F.B. & RUDI, Y.A. 2005 A model for the formation of “optimal” vortex rings taking into account viscosity. *Phys. Fluids* **17** (8), 087101.
- KRIEG, M. & MOHSENI, K. 2013 Modelling circulation, impulse and kinetic energy of starting jets with non-zero radial velocity. *J. Fluid Mech.* **719**, 488–526.
- KRIEG, M. & MOHSENI, K. 2021 A new kinematic criterion for vortex ring pinch-off. *Phys. Fluids* **33** (3), 037120.
- KRUEGER, P.S. 2005 An over-pressure correction to the slug model for vortex ring circulation. *J. Fluid Mech.* **545**, 427–443.
- LAWSON, J.M. & DAWSON, J.R. 2013 The formation of turbulent vortex rings by synthetic jets. *Phys. Fluids* **25** (10), 105113.
- LEWEKE, T., LE DIZES, S. & WILLIAMSON, C.H.K. 2016 Dynamics and instabilities of vortex pairs. *Annu. Rev. Fluid Mech.* **48** (1), 507–541.
- LIM, T.T. & NICKELS, T.B. 1995 *Vortex Rings*. Springer.
- LIMBOURG, R. & NEDIĆ, J. 2021a An extended model for orifice starting jets. *Phys. Fluids* **33** (6), 067109.
- LIMBOURG, R. & NEDIĆ, J. 2021b An extension to the universal time scale for vortex ring formation. *J. Fluid Mech.* **915**, A46.
- LIMBOURG, R. & NEDIĆ, J. 2021c Formation of an orifice-generated vortex ring. *J. Fluid Mech.* **913**, A29.
- LIMBOURG, R. & NEDIĆ, J. 2021d On the asymptotic matching procedure predicting the formation number. *Phys. Fluids* **33** (11), 117103.
- LINDEN, P.F. & TURNER, J.S. 2001 The formation of ‘optimal’ vortex rings, and the efficiency of propulsion devices. *J. Fluid Mech.* **427**, 61–72.
- MOHSENI, K. 2001 Statistical equilibrium theory for axisymmetric flows: Kelvin’s variational principle and an explanation for the vortex ring pinch-off process. *Phys. Fluids* **13** (7), 1924–1931.
- MOHSENI, K. & GHARIB, M. 1998 A model for universal time scale of vortex ring formation. *Phys. Fluids* **10** (10), 2436–2438.
- NORBURY, J. 1973 A family of steady vortex rings. *J. Fluid Mech.* **57** (3), 417–431.
- O’FARRELL, C. & DABIRI, J.O. 2012 Perturbation response and pinch-off of vortex rings and dipoles. *J. Fluid Mech.* **704**, 280–300.
- PEDRIZZETTI, G. 2010 Vortex formation out of two-dimensional orifices. *J. Fluid Mech.* **655**, 198–216.
- PIERREHUMBERT, R.T. 1980 A family of steady, translating vortex pairs with distributed vorticity. *J. Fluid Mech.* **99** (1), 129–144.

- ROSENFELD, M., KATIJA, K. & DABIRI, J.O. 2009 Circulation generation and vortex ring formation by conic nozzles. *J. Fluids Engng* **131** (9), 091204.
- ROSENFELD, M., RAMBOD, E. & GHARIB, M. 1998 Circulation and formation number of laminar vortex rings. *J. Fluid Mech.* **376**, 297–318.
- SADRI, V. & KRUEGER, P.S. 2016 Pinch-off of axisymmetric vortex pairs in the limit of vanishing vortex line curvature. *Phys. Fluids* **28** (7), 071701.
- SAFFMAN, P.G. 1978 The number of waves on unstable vortex rings. *J. Fluid Mech.* **84** (4), 625–639.
- SAFFMAN, P.G. 1992 *Vortex Dynamics*. Cambridge University Press.
- SAU, R. & MAHESH, K. 2007 Passive scalar mixing in vortex rings. *J. Fluid Mech.* **582**, 449–461.
- SCHLUETER-KUCK, K. & DABIRI, J.O. 2016 Pressure evolution in the shear layer of forming vortex rings. *Phys. Rev. Fluids* **1** (1), 012501.
- SHEPHERD, T.G. 1990 A general method for finding extremal states of Hamiltonian dynamical systems, with applications to perfect fluids. *J. Fluid Mech.* **213** (1), 573–587.
- SHUSSER, M. & GHARIB, M. 2000 Energy and velocity of a forming vortex ring. *Phys. Fluids* **12** (3), 618–621.
- STEINFURTH, B. & WEISS, J. 2020 Vortex rings produced by non-parallel planar starting jets. *J. Fluid Mech.* **903**, A16.
- THOMSON, W. 1880 Vortex statics. *Phil. Mag.* **10** (60), 97–109.
- TURKINGTON, B. 1983 On steady vortex flow in two dimensions. I. *Commun. Part. Diff. Equ.* **8** (9), 999–1030.
- VALLIS, G.K., CARNEVALE, G.F. & YOUNG, W.R. 1989 Extremal energy properties and construction of stable solutions of the Euler equations. *J. Fluid Mech.* **207**, 133–152.
- WU, J.Z., MA, H.Y. & ZHOU, M.D. 2007 *Vorticity and Vortex Dynamics*. Springer-Verlag.
- ZHAO, W., FRANKEL, S.H. & MONGEAU, L.G. 2000 Effects of trailing jet instability on vortex ring formation. *Phys. Fluids* **12** (3), 589–596.
- ZHU, J., ZHANG, G., GAO, L. & YU, S.C.M. 2023a The circulation growth of non-impulsive starting jet. *Phys. Fluids* **35** (5), 057102.
- ZHU, J., ZHANG, G., GAO, L. & YU, S.C.M. 2023b Vortex ring formation process in starting jets with uniform background co-and counter-flow. *J. Fluid Mech.* **968**, A26.